

## Behaviour of guyed transmission line structures under downburst wind loading

A. Y. Shehata<sup>†</sup>

*Atomic Energy of Canada Limited Mississauga, Ontario, Canada*

A. A. El Damatty<sup>‡</sup>

*Department of Civil and Environmental Engineering,  
The University of Western Ontario, London, Ontario, Canada*

*(Received September 16, 2006, Accepted March 26, 2007)*

**Abstract.** Past experience indicates that the majority of failures of electrical transmission tower structures occurred during high intensity wind events, such as downbursts. The wind load distribution associated with these localized events is different than the boundary layer wind profile that is typically used in the design of structures. To the best of the authors' knowledge, this study represents the first comprehensive investigation that assesses the effect of varying the downburst parameters on the structural performance of a transmission line structure. The study focuses on a guyed tower structure and is conducted numerically using, as a case study, one of the towers that failed in Manitoba, Canada, during a downburst event in 1996. The study provides an insight about the spatial and time variation of the downburst wind field. It also assesses the variation of the tower members' internal forces with the downburst parameters. Finally, the structural behaviour of the tower under critical downburst configurations is described and is compared to that resulting from the boundary layer normal wind load conditions.

**Keywords:** downbursts; microbursts; finite element; transmission line; transmission tower; wind load.

---

### 1. Introduction

A review for the cases of failure of transmission line structures that occurred in various places around the world reveals that most of those failures are attributed to high intensity wind (HIW) in the form of downbursts and tornadoes. For example, Li (2000) reported that more than 90% of transmission line failures in Australia resulted from downburst events that are usually associated with thunderstorms. The structural behaviour of an electrical transmission tower subjected to downburst loads is expected to be different than its behaviour under normal wind loads due to the following reasons:

1. A downburst wind field differs from the traditional boundary layer wind field with respect to

---

<sup>†</sup> Ph.D, Analysis and Design Engineer, E-mail: [shehataa@aecl.ca](mailto:shehataa@aecl.ca)

<sup>‡</sup> Associate Professor, Corresponding Author, E-mail: [damatty@uwo.ca](mailto:damatty@uwo.ca)

the vertical profile of the horizontal (radial) component of the wind velocity (Savory, *et al.* 2001).

2. In addition to the radial component, the downburst wind field has a vertical (axial) component (Shehata, *et al.* 2005).
3. The forces acting on a structure due to a downburst depends on the size of the event as well as the location of the structure relative to the centre of the downburst.

One of the challenges in studying the behaviour of a structure under a downburst is the prediction of the input forces acting on the structure due to this event. This necessitates the knowledge of the wind field accompanying a downburst. Two analytical approaches were developed to simulate such a field. The first approach, called the ring vortex model (Savory, *et al.* 2001, Zhu and Etkin 1986, Ivan 1986, and Vicory 1992), simulates the downburst as descending air shaft that causes ring vortex prior to approaching the ground surface. In the second approach, the downburst is simulated as an impinging jet that causes a horizontal (radial) and a vertical (axial) flow after touching down the ground (Vicory 1992, Holmes and Oliver 2000). This impinging jet approach has been recently used by Hangan, *et al.* (2003) in a computational fluid dynamic analysis to provide a complete time history representation for the velocity field associated with a downburst. This time history data is the basis of the input forces applied in the current study. Recently, Chay, *et al.* (2006) used a CFD analysis to generate a steady state model of non-turbulent downburst field based on the simulation of 30 downburst scenarios. A turbulent model was added in this study to the main component of the wind field.

Despite the fact that many structures failed under localized wind events in general and downburst in particular, little attempts were made to conduct structural analysis research under such type of loads. Chen and Letchford (2003) studied the response of the Commonwealth Aeronautical Advisory Research Council (CAARC) building to downburst wind loading. Savory, *et al.* (2001) carried out a research study on a lattice transmission tower under tornadoes and downburst wind loadings. In this study, a modified form of a tornado loading model was utilized to estimate the downburst-induced wind loads. The behaviour of the tower was studied under a specific downburst configuration. Neither the vertical (axial) component of the downburst wind field nor the downburst forces acting on the conductors were considered in the study. Shehata, *et al.* (2005) presented a numerical approach to predict the behaviour of transmission line structures under downburst loads. The input wind field data is based on the results of the computational fluid dynamic (CFD) analysis conducted by Hangan, *et al.* (2003). An experimental validation of this wind field data was also conducted by Hangan, *et al.* (2003). The approach used to transform the downburst velocity field into forces acting on a transmission line was described in detail by Shehata, *et al.* (2005). Structural modelling of both the transmission tower and the attached conductors were conducted in this study. Only the main component of the downburst wind loading was considered in this study. The current study represents an extension to the work conducted by Shehata, *et al.* (2005). To the best of the authors' knowledge, it represents the first comprehensive study conducted to assess the behaviour of a transmission line structure under downbursts while taking into consideration the variability of the downburst characteristics. The study is conducted numerically using, with some minor modifications, the numerical model developed by Shehata, *et al.* (2005). The objectives of the current study are as follows:

1. Provide the reader with an understanding about the spatial and time variations of the velocity wind field associated with a downburst acting on a real transmission tower.
2. Assess the effect of the variation of the downburst characteristics on the internal forces

developing in members of a transmission tower.

3. Describe the structural behaviour of guyed transmission towers under critical downburst configurations and compare them to the behaviour under normal wind conditions.

A generic guyed tower, which previously failed under a downburst event that occurred in Winnipeg, Manitoba, Canada 1996 (Transmission and Civil Design Department, Manitoba Hydro 1999), was used to conduct the study. A brief description of the considered tower/line structure is first introduced in the paper. A summary of the modeling technique and the steps used in the analysis are then provided. This is followed by a presentation for the spatial and time variations of both the radial and vertical components of the downburst velocity fields acting on various location of the structure. Results of the extensive parametric study are then introduced followed by a description of the structural behaviour. Finally, a discussion for the major conclusions that can be drawn from this study is provided.

## 2. Modelling of the transmission line system

One of the typical towers used in Manitoba Hydro electrical transmission line systems is considered in this study. According to Manitoba Hydro classification, the tower is labelled as Type A-402-0 (Engineering and Construction, Manitoba Hydro 1991). A schematic of the tower geometry is provided in Fig. 1. It is also classified as a guyed tower since in addition to the restraint at the base support, the displacement of the tower is constrained by the four guys connected at an elevation 35.18 (m) relative to the ground. As shown in Fig. 1, the tower is divided to seven zones.

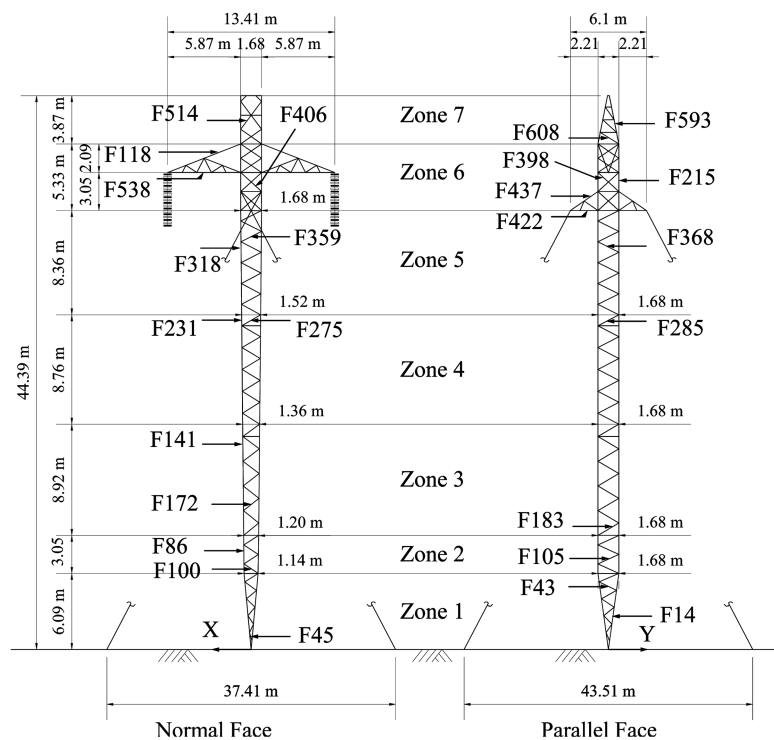


Fig. 1 Geometry of the modeled lattice transmission tower type A-402-0

The intersection between two zones represents a location for a splice between two members of the tower legs. The total height of the tower is 44.39 (m). The conductors and the ground wires are connected to the tower at elevations of 38.23 (m) and 44.39 (m), respectively. The geometric and material properties of the conductors and ground wires are provided by Shehata, *et al.* (2005).

### 3. Modeling and analysis techniques

A brief description for the modelling and analysis techniques used in the current study is provided in this section. For more information, the reader is referred to Shehata, *et al.* (2005).

#### 3.1. Downburst wind field based on CFD analysis

As mentioned above, the input wind field data for downburst used in this study is based on a CFD analysis that was conducted and experimentally validated by Hangan, *et al.* (2003). This wind field data correspond to specific values for the jet diameter  $D_{jm}$  and the jet velocity  $V_{jm}$ . The CFD analysis does not consider the translation component of the downburst. The velocity field resulting from the CFD analysis is described using a radial (horizontal) component  $V_{mRD}$  and an axial (vertical) component  $V_{mAX}$ . At a certain point in space, these two components are functions of the variables  $r_m$  and  $z_m$ , which represent the cylindrical coordinates of the point of interest relative to the centre of the downburst. These two velocity components also vary with time, i.e., they are given as time history series.

A procedure to scale-up these wind field data in order to determine the velocity profile acting on a full-scale tower due to a real downburst event is described by Shehata, *et al.* (2005). Accordingly, at an arbitrary point of the structure, two velocity components  $V_{RD} = V_{RD}(D_{Jf}, V_{Jf}, r_f, Z_f, t_f)$  and  $V_{AX} = V_{AX}(D_{Jf}, V_{Jf}, r_f, Z_f, t_f)$  can be evaluated, where  $V_{RD}$  and  $V_{AX}$  are the radial (horizontal) and the axial (vertical) velocities of the wind field data at this point, respectively. As shown above, the velocity components  $V_{RD}$  and  $V_{AX}$  depend on the downburst diameter  $D_{Jf}$ , its descending velocity  $V_{Jf}$  and the coordinates  $r_f$  and  $Z_f$  which represent the cylindrical coordinates of the point of interest relative to the centre of the downburst.

#### 3.2. Structural modelling

This subsection highlights the main features that are taken into consideration in the numerical modelling of the transmission line/tower assembly.

##### 3.2.1. Modelling of conductors

The study conducted by Shehata, *et al.* (2005) revealed that it is sufficient to consider six conductor spans (three from each side) in order to estimate accurately the forces acting on a tower. The conductors are modelled using a two-dimensional curved beam element (Koziey and Mirza 1994, and Gerges and El Damatty 2002) that considers the non-linear behaviour associated with the large deformation experienced by the conductors. Two separate sets of analyses are conducted to determine the responses of the conductors to the forces associated with the radial and axial components of the velocity field, respectively. In the first analysis (due to radial forces), the conductors are modelled in a horizontal plane, while in the second analysis (due to axial forces), the conductors are modelled in a vertical plane. In the second set of analyses, the curved geometry of the conductors resulting from

the sag and the associated pre-tension force are considered in the numerical modelling. The boundary conditions at the end of each conductor span were simulated using a system of springs that represents the stiffness provided by both the tower and the insulator strings at these locations. Detailed derivation of this spring system is provided by Shehata, *et al.* (2005).

### 3.2.2. Modelling of tower and guys

Both the tower members and the guys were modelled using three-dimensional space frame elements having two nodes and six degrees of freedom (three translational and three rotational) per node. The large pre-stressing forces typically applied to the guys increase significantly their stiffness and accordingly the behaviour of the guys can be simulated using a linear analysis.

### 3.3. Sequence of analysis

A downburst is defined by its jet diameter  $D_{Jf}$  and its jet velocity  $V_{Jf}$ . Also, the forces resulting from a downburst and acting on a transmission line/tower system depend on the two geometric parameters  $r_f$  and  $\theta_f$ , which represent the location of the centre of the downburst relative to the centre of the tower (see Fig. 2). The parameters  $V_{Jf}$ ,  $D_{Jf}$ ,  $r_f/D_{Jf}$  and  $\theta_f$  will be defined as the downburst characteristics. Since the frequency of the tower is much higher than the downburst loading frequency, Shehata, *et al.* (2005) has shown that the dynamic effects of both the tower and the conductors have a very minor influence on the response of the tower. Consequently, the time increment analysis can be conducted in a quasi-static manner. For a specific downburst configuration, the following steps are conducted to estimate the internal forces resulting from this event.

1. Knowing  $r_f$ ,  $\theta_f$  and the Cartesian coordinates of nodal points of both the tower and the conductors, the cylindrical coordinates of those points relative to the centre of the downburst ( $r_{fa}$ ,  $\theta_{fa}$ ,  $Z_{fa}$ ) can be evaluated. The subscript 'a' denotes the nodal point of interest. The radial and axial velocities  $V_{RD}$  and  $V_{AX}$  at these nodal points are then evaluated using the procedure described in section 3.1.
2. Using these velocity components, the nodal forces acting on both the tower and the conductors are then evaluated using the methodology described in detail by Shehata, *et al.* (2005).

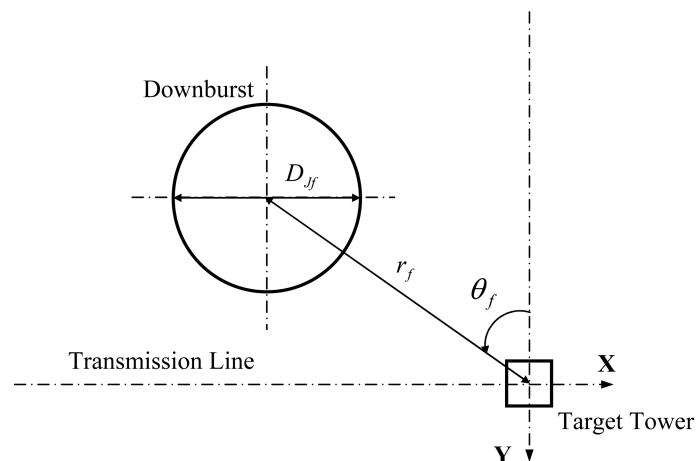


Fig. 2 Downburst parameters employed in the parametric study

- Two sets of non-linear analyses are conducted for the conductors due to the effect of the radial (horizontal) and axial (vertical) velocity components, respectively. It should be mentioned that the vertical component of the downburst loading acting on the conductors has shown to have a very low intensity and practically its effect can be neglected compared to the effect of the radial (horizontal) component. This justifies decoupling the analyses under vertical and horizontal loads. Reaction forces obtained from these analyses are reversed and then applied on the tower at the conductors/tower intersection points. In addition, the tower is subjected to the downburst forces acting on its nodes. A linear analysis is conducted for the tower under this assembly of forces that leads to an estimate for the time history variations of the internal forces acting on various members of the tower due to the specific downburst configuration.

#### 4. Downburst wind field profile

The purpose of this section is to assist the reader in visualizing the spatial and time variations of the wind velocity field resulting from various downburst configurations. Fig. 3 shows the time history variations for the radial velocity at an elevation of approximately 32.0 (m) above the ground. The figure shows the variations corresponding to three different values of the jet diameter  $D_{Jf}$ . In the three plots shown in Fig. 3(a), the location of the point at which the velocity is provided was selected such that the ratio  $r_f/D_{Jf}$  is kept constant at a value of 1.20. The three plots show a typical trend that has a maximum peak, followed by a minimum peak, followed by a constant value. The symbols  $t_1$  and  $t_2$  will denote the time instants at which the maximum and minimum peaks occur, respectively. The symbols  $V_{RD\max}$ ,  $V_{RD\min}$  and  $V_{RD\text{cons}}$  are used to identify the maximum peak, the minimum peak, and the constant values, respectively. It can be concluded from the figure that for the same  $r_f/D_{Jf}$  ratio, the variation of  $V_{RD\max}$  and  $V_{RD\min}$  with  $D_{Jf}$  is very small, while the variation of  $V_{RD\text{cons}}$  with  $D_{Jf}$  is more pronounced. It can also be noticed that the values of  $t_1$  and  $t_2$  vary almost linearly proportional to the diameter of the jet. The analysis indicates that the value of  $t_1$  ranges between  $(0.196 \sim 0.231) D_{Jf}$ , while the value of  $t_2$  ranges between  $(0.238 \sim 0.266) D_{Jf}$ . As a demonstration, the value of  $t_1$  almost doubled when  $D_{Jf}$  is varied from 250 (m) to 500 (m) and is magnified by a factor of 4 when  $D_{Jf}$  is varied from 250 (m) to 1000 (m). Similar trend is shown for  $t_2$ . Same graphs are shown in Fig. 3(b) for a  $r_f/D_{Jf}$  value of 1.60. Similar conclusions can be drawn from this figure. Fig. 4 shows the vertical profile of  $V_{RD\max}$  (at  $t = t_1$ ) for different  $r_f/D_{Jf}$  and

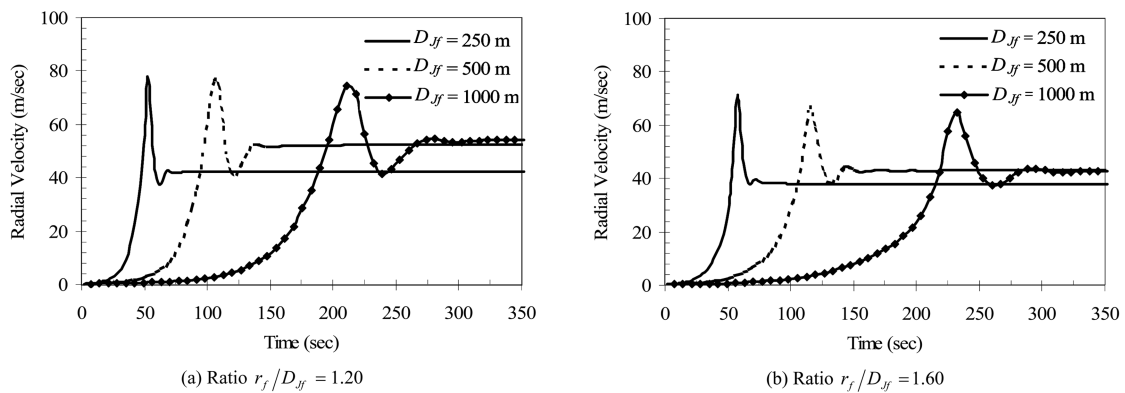


Fig. 3 Time history of the downburst radial velocity for different  $r_f/D_{Jf}$  ratios

various  $D_{Jf}$  values. It can be seen from the figure that a downburst with configurations  $D_{Jf} = 250$  (m) and  $r_f/D_{Jf} = 1.20$  would produce the largest values of horizontal forces acting on the tower.

Similar observations can be noticed in Fig. 6 for the axial velocity component. Fig. 5 shows the time history variation of the axial velocity at an elevation of 32.0 (m) above the ground. Figs. 5(a) and 5(b) illustrate the time history variations corresponding to three different values of the jet diameter  $D_{Jf}$  and for two values of  $r_f/D_{Jf}$ . In Fig. 5(a), the profile is provided at a location just below the centre of the jet of the downburst, i.e., at ratio  $r_f/D_{Jf} = 0.0$ . The symbols  $V_{AXmax}$ ,  $V_{AXmin}$  and  $V_{AXcons}$  are used to identify the maximum peak, the minimum peak, and the constant values, respectively. Meanwhile,  $t_1$  and  $t_2$  denote the time instants at which the maximum and minimum peaks occur, respectively. The three plots of the figure show that the values of  $V_{AXmax}$ ,  $V_{AXmin}$  and  $V_{AXcons}$  decrease with the increase of the jet diameter  $D_{Jf}$ . In fact, these values are almost inversely proportional to the jet diameter. For example, the value of  $V_{AXmax}$  decreased by a factor of 2 when  $D_{Jf}$  is varied from 250 (m) to 500 (m) and decreased by a factor of 4 when  $D_{Jf}$  is varied from 250 (m) to 1000 (m). Same trend is noticed for  $V_{AXmin}$  and  $V_{AXcons}$ . The values of  $t_1$  and  $t_2$  follow an

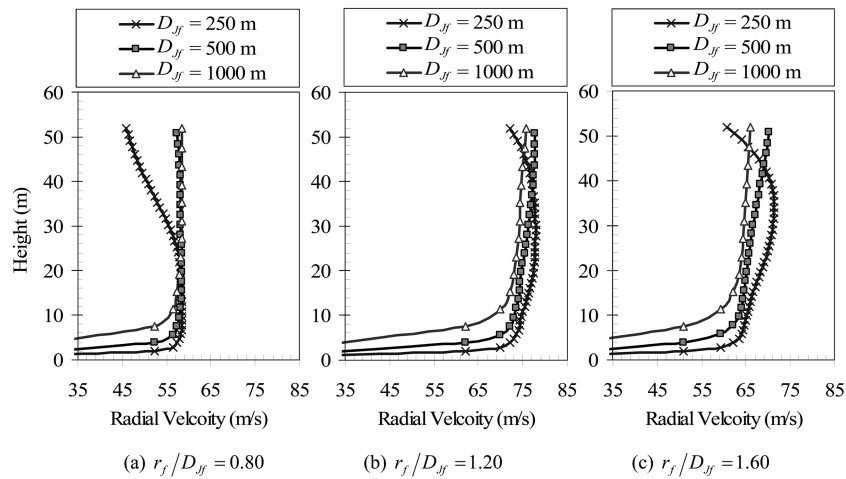


Fig. 4 Vertical profile of downburst radial velocity for different  $r_f/D_{Jf}$  ratios

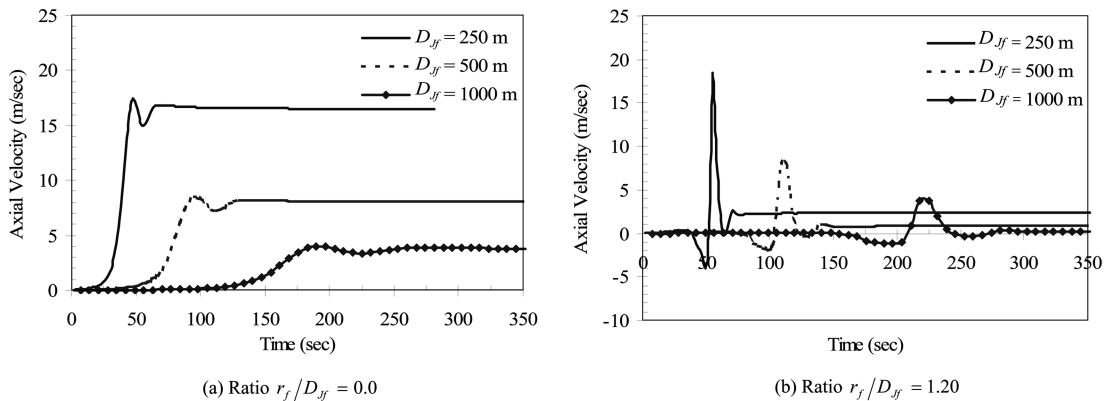


Fig. 5 Time history of the downburst axial velocity for ratio  $r_f/D_{Jf} = 1.20$

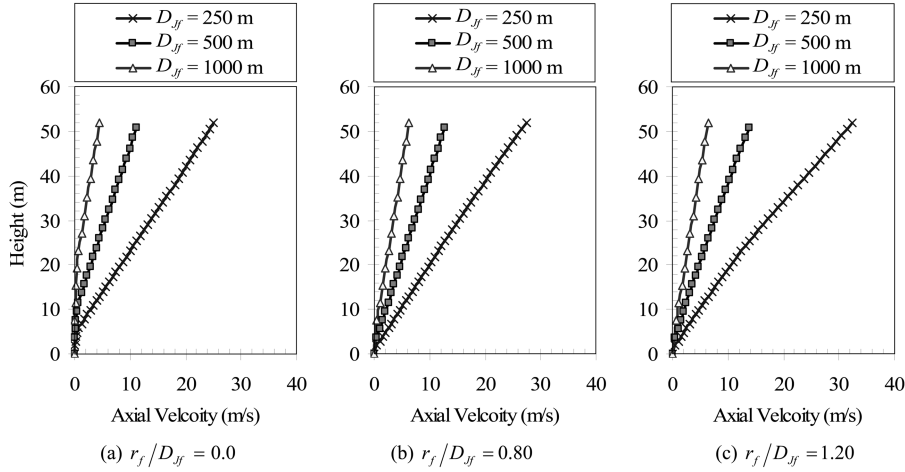


Fig. 6 Vertical profile of downburst axial velocity for different  $r_f/D_{Jf}$  ratios

opposite trend, as they are linearly proportional to the jet diameter. The analysis indicates that the value of  $t_1$  ranges between  $(0.203 \sim 0.224) D_{Jf}$ , while the value of  $t_2$  ranges between  $(0.196 \sim 0.245) D_{Jf}$ . Fig. 5(b) shows the time history variation of the axial velocity at a location corresponding to  $r_f/D_{Jf} = 1.20$  for different values of the jet diameter  $D_{Jf}$ . It can also be noticed from the figure that  $V_{AX\max}$ ,  $V_{AX\min}$ , and  $V_{AX\cons}$  are following the same trend observed in Fig. 5(a) for  $r_f/D_{Jf} = 0.0$ . In comparison with the  $r_f/D_{Jf} = 0.0$  case, Fig. 5(b) indicates that for  $r_f/D_{Jf} = 1.20$ , the values of  $V_{AX\max}$  has slightly increased while the values of  $V_{AX\min}$  and  $V_{AX\cons}$  have both decreased significantly. Also, the trend for  $r_f/D_{Jf} = 1.20$  has changed as the minimum value precedes the maximum one in terms of the time of occurrence. Fig. 6 shows the vertical profile of the maximum axial velocity  $V_{AX\max}$  (at  $t = t_1$ ) for different  $r_f/D_{Jf}$  and various  $D_{Jf}$  values. It is noticed from the figure that the velocity profile associated with  $\theta_f = 250$  (m) provides the largest values and the absolute maximum occurs at  $r_f/D_{Jf} = 1.20$ . It is also noticeable that the magnitudes of the axial velocities are much lower than those of the radial velocities.

## 5. Parametric study

Results of an extensive parametric study conducted using the approach outlined in section 3 are presented in this section. The objective of this parametric study is to assess the variations of the internal forces developing in members of various zones of the transmission tower with the downburst characteristics. As mentioned earlier, the characteristics defining the effect of a downburst on a structure are  $D_{Jf}$ ,  $V_{Jf}$ ,  $r_f/D_{Jf}$  and  $\theta_f$ , respectively. No attempt was done in the study to vary the jet velocity  $V_{Jf}$  since it is obvious that the internal forces will increase monotonically with an increase in  $V_{Jf}$ . A single value for  $V_{Jf} = 70$  (m/s), which represents the extreme wind speed value recorded in field observation of downburst events (Savory, *et al.* 2001), is used. The following values of  $D_{Jf} = 250, 500, 1000$  and  $2000$  (m) were used in the parametric study. For each jet diameter, the ratio  $r_f/D_{Jf}$  varied between 0 and 2.20 using an increment of 0.20. Due to double symmetry, the downburst was assumed to be located within one quadrant and, accordingly, the value of  $\theta_f$  varied between  $0^\circ$  and  $90^\circ$ . For each combination of  $D_{Jf}$  and  $r_f/D_{Jf}$ , seven values of  $\theta_f = 0^\circ, 15^\circ, 30^\circ, 45^\circ, 60^\circ, 75^\circ$  and  $90^\circ$  were assumed, respectively. As such, a total number of 336

analyses were conducted in this study. Each time history analysis involved 240 time steps, which represents the total number of increments provided by the CFD analysis. After those 240 increments, the downburst field reaches its steady state and therefore, further consideration of time increments would have no benefit. Following the steps described in section 3, for each downburst configuration, the finite element program predicts the axial forces in all members of the tower at each time increment. For each member, the absolute maximum force resulting from the entire time history analysis and corresponding to each downburst configuration was evaluated. The variations of the axial forces with the downburst parameters were provided in a graphical form for selected members.

As shown in Fig. 1, the tower is divided into seven zones. The first five zones are located below the supporting guys. Zone (6) represents the cross-arms area and zone (7) is the upper part of the tower. The absolute maximum axial forces resulting from the large parametric study at specific members of each zone are provided in Table 1. For each member, the downburst parameters ( $D_{Jf}$ ,  $r_f$ / $D_{Jf}$  and  $\theta_f$ ) corresponding to the maximum force are provided in the table. The time instant at which the maximum force occurs is also given in the table. For each zone, the results are provided at a leg member, and two diagonal members denoted as diagonal (I) and diagonal (II), which represent a member located in a plane parallel to the transmission line and a member located in a plane perpendicular to the transmission line, respectively. In addition, for zone (6), the maximum axial forces developing in upper and lower chord members of the conductors cross-arms and the guys cross-arms are presented.

It should be noted that the value of  $\theta_f = 0^\circ$  corresponds to the situation where the centre of the downburst and the centre of the tower are located in a plane perpendicular to the transmission line. Meanwhile, the situation for  $\theta_f = 90^\circ$  occurs when the centre of the downburst and the centre of the tower are located in a plane parallel to the transmission line. Intermediate situations occur for  $0^\circ \leq \theta_f \leq 90^\circ$ . In the same table, the maximum axial forces resulting from applying the ASCE No. 74 guidelines (1991) are provided for the considered members. When applying the ASCE No. 74 guidelines (1991), the reference velocity at 10 meter height was selected in such a way that it matches the corresponding value associated with a downburst having a jet velocity  $r_f = 70$  (m/s). The following general conclusions can be drawn from the results provided in the table.

- Zones (1) to (5) exhibit almost the same behaviour as the maximum axial forces in each category of members (Leg, Diagonal (I) and Diagonal (II)) occur at the same downburst configurations. This is true for all cases with the exception of diagonal member (II), where the critical value of  $D_{Jf}$  varied between 250 (m) in zones (1) and (2) and 500 (m) in zones (3) to (5).

- For zones (6) and (7), the maximum axial forces in each category of members (Leg, Diagonal (I) and Diagonal (II)) located in main body of the tower happen at different downburst configurations. For members located in the conductors and guys cross-arms, there is almost a specific critical downburst configuration for each cross-arm.

- The maximum axial forces in the leg members of zones (1) to (4) due to downburst loading exceed those due to normal wind loading by a percentage that ranges between 5.70% and 12.50%. However, for the leg members located in zones (5) and (6), the maximum axial forces due to normal wind loading exceed those due to downburst loading by about 40%. The reason behind that observation will be explained in a later section of this paper.

- The axial forces in the conductors cross-arm and the upper chord of the guys cross-arm due to downburst wind loading exceed significantly those due to normal wind loading.

- In zones (1) to (5) and zone (7), the axial forces in the diagonal member (I) due to downburst and normal wind loads are almost equal. However, for diagonal member (I) of zone (6), the axial

Table 1 Results of the parametric study due to downburst wind loading and ASCE No.74 guidelines loading

	Member		Downburst Wind Loading				ASCE	
	No.	Type	$D_{jf}$ (m)	$r_f/D_{jf}$	$\theta_f$	Time (sec)	Axial Force (kN)	Axial Force (kN)
Zone 1	F14	Leg	250	1.20	90°	52.73	88.50	83.75
	F43	Diagonal (I)	250	1.20	90°	52.73	2.04	2.41
	F45	Diagonal (II)	250	1.20	0°	52.73	10.30	5.58
Zone 2	F86	Leg	250	1.20	90°	52.73	109.80	102.15
	F105	Diagonal (I)	250	1.20	90°	52.73	20.65	19.02
	F100	Diagonal (II)	250	1.20	0°	52.73	9.51	1.89
Zone 3	F141	Leg	250	1.20	90°	52.73	171.80	156.86
	F183	Diagonal (I)	250	1.20	90°	52.73	17.78	16.08
	F172	Diagonal (II)	500	1.20	0°	105.46	2.45	6.60
Zone 4	F231	Leg	250	1.20	90°	52.73	174.80	155.41
	F285	Diagonal (I)	250	1.20	90°	52.73	7.36	7.73
	F275	Diagonal (II)	500	1.20	0°	105.46	22.85	25.65
Zone 5	F318	Leg	250	1.20	90°	52.73	131.80	213.02
	F368	Diagonal (I)	250	1.20	90°	52.73	16.60	16.25
	F359	Diagonal (II)	500	1.20	0°	105.46	31.00	32.70
Zone 6	F215	Leg	250	1.80	45°	54.49	56.60	108.44
	F398	Diagonal (I)	500	1.40	45°	105.46	46.10	14.95
	F406	Diagonal (II)	1000	1.20	0°	210.91	53.70	63.10
	F437	Upper Chord	500	1.40	30°	108.97	143.00	92.36
	F422	Lower Chord	500	1.40	30°	108.97	126.80	142.57
	F118	Upper Chord	1000	1.60	30°	224.97	98.70	3.11
	F538	Lower Chord	1000	1.60	30°	224.97	128.40	38.88
Zone 7	F593	Leg	250	1.80	45°	54.49	52.41	12.39
	F608	Diagonal (I)	500	1.20	90°	105.46	2.92	2.61
	F514	Diagonal (II)	500	1.40	30°	108.97	22.91	11.22

forces due to downburst wind exceed those due to normal wind by a factor of 3.

- In zones (1), (2) and (7) the axial forces in diagonal (II) members due to downburst wind loading exceed those due to normal wind loading, while the reverse occurs for the rest of the zones. This observation can be explained through investigating the shear force diagram along the tower height, which will be discussed in a later section of this paper.

A discussion about the variations of the axial forces with the three downburst parameters members is provided below for different zones.

### **Zones (1) to (5)**

In presenting the variation of the forces resulting from the parametric study with a specific

variable, the other two variables were kept constant. For example, for member *F14*, the variation of the member's force with  $\theta_f$  is presented for specific values of  $D_{Jf}$  and  $r_f/D_{Jf}$  set equal to 250 (m) and 1.20, respectively. According to Table 1, these two values lead to maximum forces in member *F14*. Since members of zones (1) to (5) were shown to exhibit almost the same behaviour, typical plots are provided to illustrate the variation of axial forces in these zones. Zone (6) was shown to have a unique behaviour and, therefore, plots for specific members in this zone are provided separately.

Fig. 7 shows the typical variation of the axial forces for leg, diagonal (I) and diagonal (II) members for zones (1) to (5) with the downburst parameters. Fig. 7(a) indicates a slight variation of the leg member force with the angle  $\theta_f$  with a maximum value occurring at  $\theta_f = 90^\circ$ . A comparison between the two cases of  $\theta_f = 0^\circ$  and  $\theta_f = 90^\circ$  will be carried out later and will provide an explanation for the trend shown in this figure. The variation of the axial forces in the diagonal members with  $\theta_f$  is more significant, as shown in Figs. 7(b) and 7(c). As one would expect, a maximum force develops in each diagonal member when the plane containing the centres of the downburst and the tower is parallel to that member. Fig. 7 also shows the change of the axial forces in the three member categories with the ratio  $r_f/D_{Jf}$ . It is clear that for zones 1 to 5, maximum forces occur when the location of the downburst relative to the tower  $r_f$  satisfies the relation  $r_f/D_{Jf} = 1.20$ . A monotonic decrease in the axial forces with the increase in the downburst diameter  $D_{Jf}$  is shown in Fig. 7 for the three member categories.

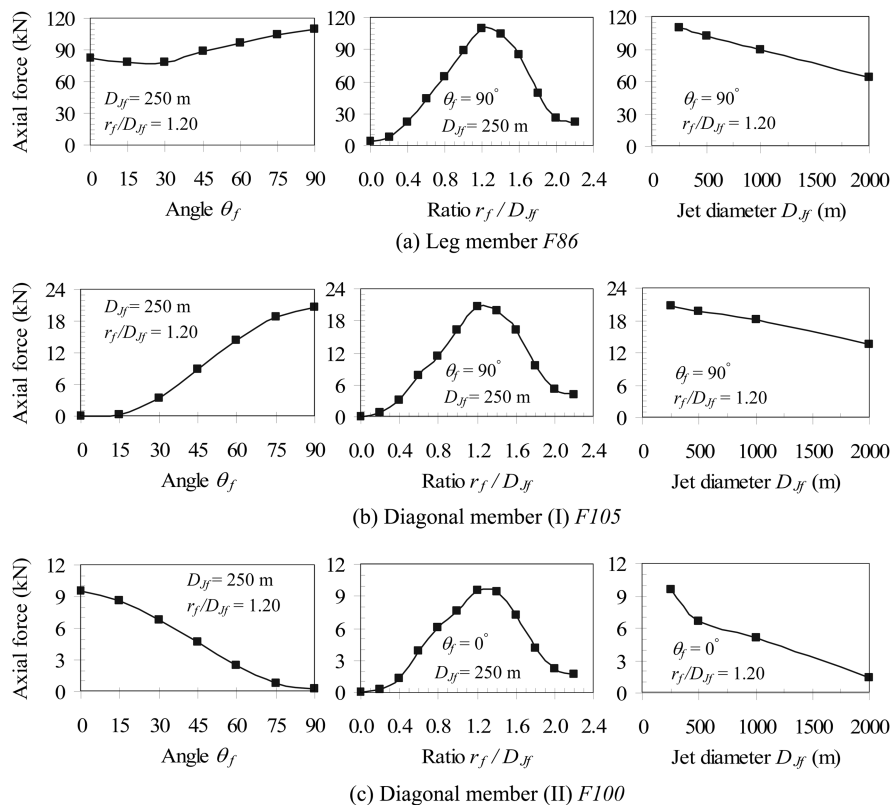


Fig. 7 Variation of axial forces in zones (1) to (5) with downburst parameters

**Zone (6)**

Forces developing in the three regions of zone (6) are presented herein. Members *F215*, *F398* and *F406* are all located within the main body of the tower and represent leg, diagonal (I) and diagonal (II) members, respectively. As shown in Fig. 1, members *F437* and *F422* are connected to the guys that support the tower. Meanwhile, members *F118* and *F538* are attached to the insulator string that carries the conductors.

The variations of the maximum axial forces in members *F215*, *F398* and *F406* with the downburst parameters are provided in Fig. 8. The figure indicates that the trend of variation with  $\theta_f$  in this zone is different than that of zones (1) to (5), where absolute maximum values were shown to occur at either  $\theta_f = 0^\circ$  or  $\theta_f = 90^\circ$ . As shown in the plots, the absolute maximum forces for the leg and the diagonal (I) members occur at  $\theta_f = 45^\circ$ . At this value of  $\theta_f$ , the conductors at both sides of the tower are subjected to unbalanced loads, which contribute to the large forces associated with this angle. Further elaboration on this point will be provided in a later section of this paper. Fig. 8 indicates that the cases where the maximum forces occur at intermediate value of  $\theta_f$  (i.e.  $\theta_f \neq 0^\circ$  and  $\theta_f \neq 90^\circ$ ), the corresponding  $r_f/D_{jf}$  ratio is different than the value of 1.20 that was consistently obtained for zones (1) to (5). Maximum axial forces occurred at  $r_f/D_{jf} = 1.80$  and 1.40 for the leg and diagonal (I) members, respectively. Again, unlike the behaviour of zones (1) to (5), where a monotonic decline was typically associated with an increase in  $\theta_f$ , Fig. 8 indicates peak values corresponding to specific values of  $D_{jf}$ . These correspond to 500 (m) and 1000 (m) for the diagonal

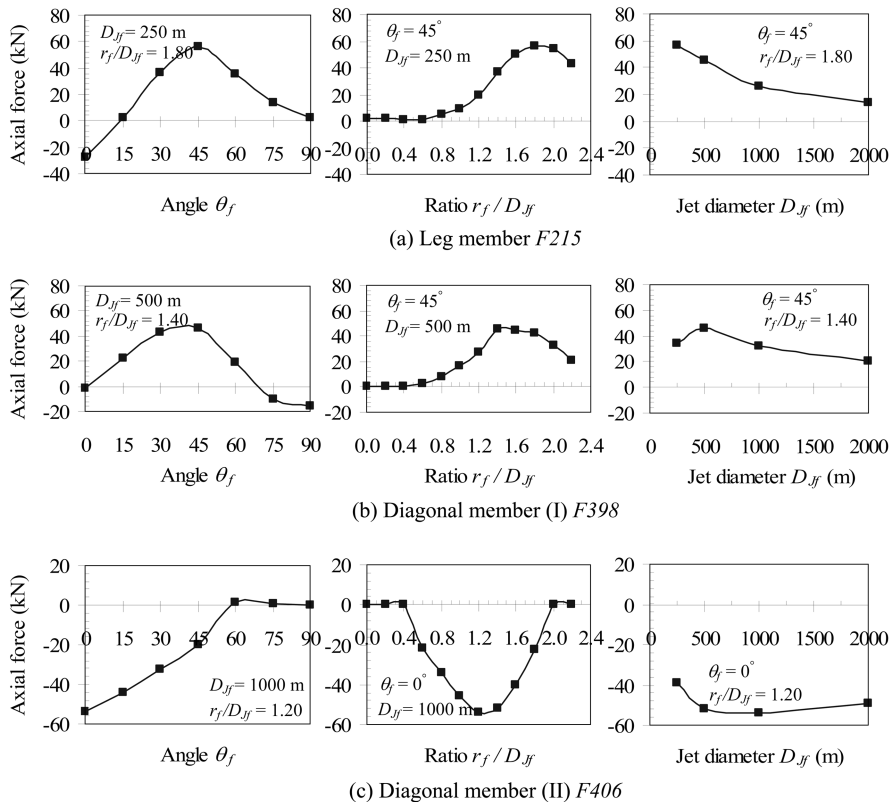
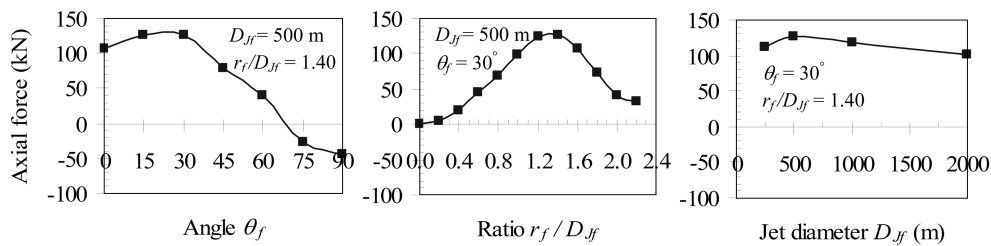


Fig. 8 Variation of axial forces in zone (6) with downburst parameters

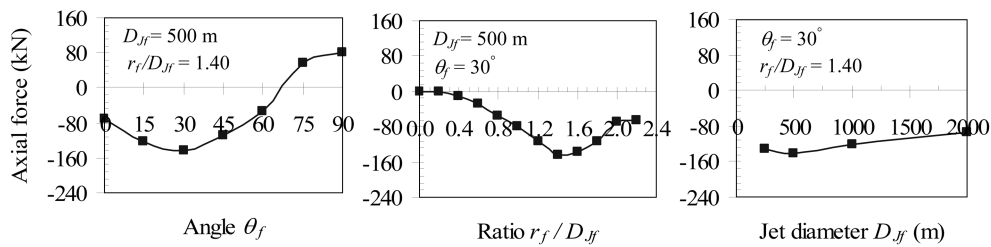
(I) and diagonal (II) members, respectively. The variation of the axial forces for the members connected to the guys and the conductors are provided in Fig. 9. The following conclusions can be drawn from these figures:

An intermediate value of  $\theta_f = 30^\circ$  leads to maximum forces in all members. Again, this configuration corresponds to a case of uneven loading acting on the conductors located at both sides of the tower.

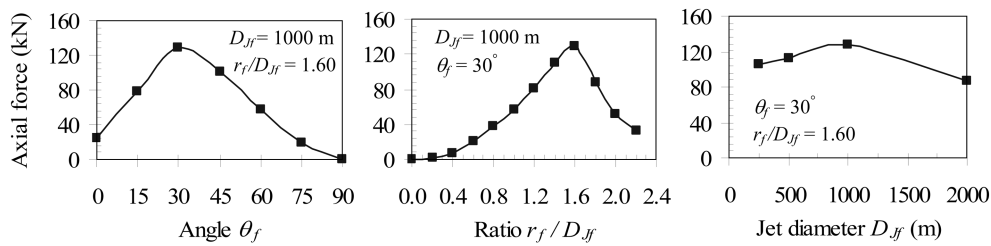
Maximum forces occur at  $r_f/D_{Jf}$  ratios that are different than the value of 1.20. Critical  $r_f/D_{Jf}$



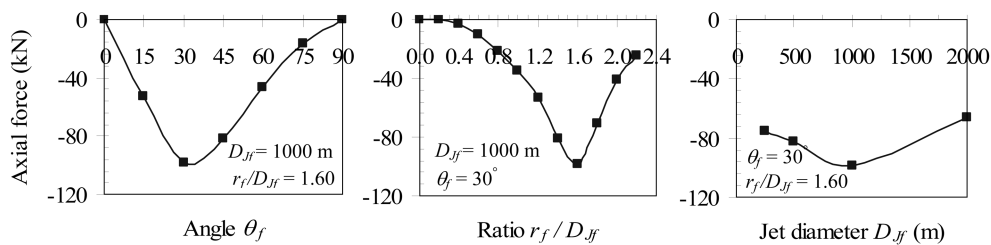
(a) Guys' cross-arm member (lower chord) F422



(b) Guys' cross-arm member (upper chord) F437



(c) Conductors' cross-arm member (lower chord) F538



(d) Conductors' cross-arm member (upper chord) F118

Fig. 9 Variation of axial forces in zone (6) (guys and conductors cross-arms) with downburst parameters

values of 1.40 and 1.60 are obtained for members connected to the guys and the conductors, respectively.

Unlike the trend obtained for members of zones (1) to (5), a peak force is shown at a specific value of  $D_{Jf}$ . This value varied between 500 (m) for the guys cross-arms and 1000 (m) for the conductors cross-arms.

### Zone (7)

The trend of variation of the forces in zone (7) shows somehow similar behaviour as zone (6) characterized by an intermediate critical value of  $\theta_f$ , a critical  $r_f/D_{Jf}$  value exceeding 1.20, and a peak value at a specific  $D_{Jf}$  configuration. Due to space limitation, plot describing such variations will not be provided in this paper.

## 6. Behaviour of transmission tower under downburst and normal wind loadings

The purpose of this section is to illustrate the behaviour of guyed transmission towers due to loading resulting from the critical downburst configurations and to compare it to the behaviour under normal wind loads. Three downburst configurations, which according to the results provided in Table 1 are shown to be critical, are considered in this section.

### 6.1. Case I ( $\theta_f = 0^\circ$ )

The following downburst configuration  $D_{Jf} = 250$  (m),  $r_f/D_{Jf} = 1.20$ ,  $\theta_f = 0^\circ$  and  $V_{Jf} = 70.0$  (m/s) is considered in this case. As shown in Table 1, this configuration leads to maximum forces in the diagonal (II) members of zones (1) and (2). A simulation for the tower as a beam supported using springs simulating the guys stiffness and restrained from motion at its bottom edge is shown in Fig. 10(a).

The arrows shown in Fig. 10(a) represent the point loads acting at various locations along the height of the tower due to a downburst having the above mentioned characteristics. Also shown in the figure, the forces at points C and D resulting from the downburst loads acting on the conductors. It should be noted that, except for the conductors, the forces shown in Fig. 10(a) are drawn to scale using the scaling ratio provided in the figure. Similar forces resulting from normal wind loads and calculated using ASCE No.74 guidelines (1991) are provided in Fig. 10(a). With the exception of the conductors, the forces are drawn using the same scale applied in Fig. 10(a). A comparison between the downburst and the normal wind profiles indicates that the forces acting on the tower itself are almost equal for both cases. On the other hand, the forces acting on the conductors due to normal wind loading exceed significantly those due to downburst loading. This can be explained in a view of the conclusion reached in section 4 that the radial component of the velocity profile decreases significantly when the ratio  $r_f/D_{Jf}$  exceeds 1.20. In the considered case, the relative distance  $r_f$  between the centres of the downburst and the tower satisfies the ratio  $r_f/D_{Jf} = 1.20$ . As for the conductors, the effective value of  $r_f/D_{Jf}$  at different points will exceed 1.20 and therefore, smaller forces act at these locations. Fig. 10(b) shows the displacement profile as well as the variations of the bending moment and shear force along the height of the equivalent beam due to both the downburst and normal wind loads, respectively. The large conductor forces associated with the normal wind load case led to larger values for the deflection, the negative bending moment and the shear force at the cantilever portion of the beam. Only at the lower portion

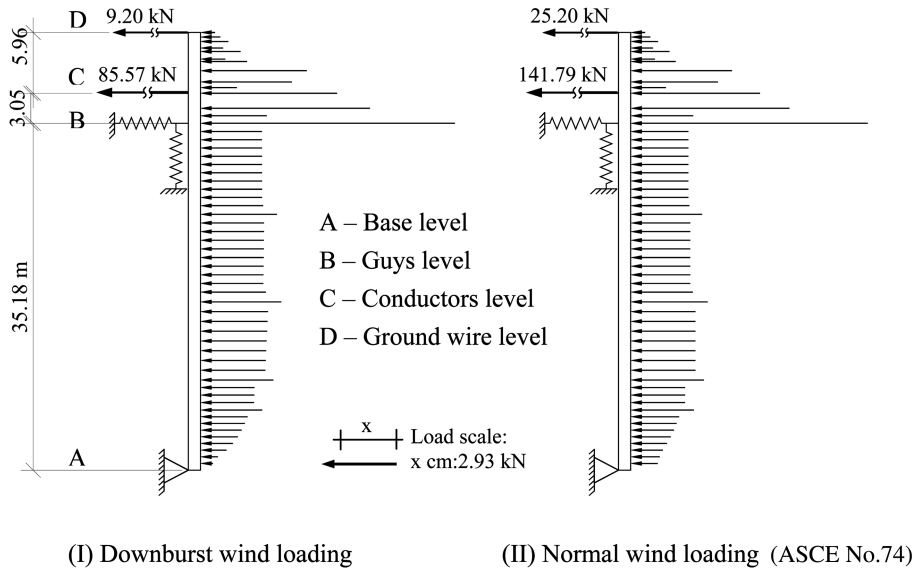


Fig. 10(a) Vertical profile of wind loading at  $\theta_f = 0^\circ$

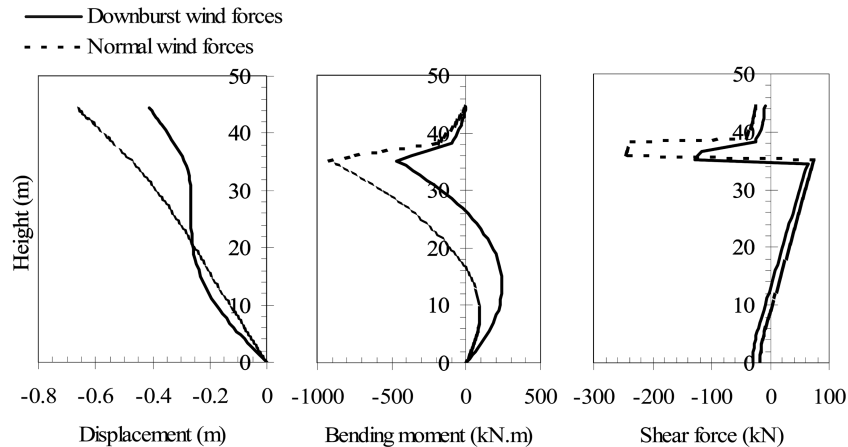


Fig. 10(b) Structural behaviour at  $\theta_f = 0^\circ$

of the tower, the bending moment values due to downburst loading exceed those due to normal wind loading. The values of the bending moment reflect the magnitude of axial forces acting on the leg members. According to Table 1, maximum forces in the leg members are governed by downburst configurations that are different than the case of  $\theta_f = 0^\circ$ . The considered downburst configuration is important for diagonal (II) members of zones (1) to (5) as Table 1 shows that the maximum forces in all these members correspond to  $\theta_f = 0^\circ$  and  $r_f/D_{ff} = 1.20$ . The values of the shear forces shown in Fig. 10(b) will reflect the magnitude of forces in these diagonal (II) members. The diagram shown in Fig. 10(b) indicates that with the exception of the bottom 12.0 (m), the shear forces due to normal wind loads exceed those due to the downburst loads. This observation coincides with the results shown in Table 1, which indicates that for zones (1) and (2), the forces in diagonal (II) members are governed by the downburst loads.

6.2. Case II ( $\theta_f = 90^\circ$ )

This downburst configuration is defined by the following parameters;  $D_{Jf} = 250$  (m),  $r_f/D_{Jf} = 1.20$ ,  $\theta_f = 90^\circ$  and  $V_{Jf} = 70.0$  (m/s). According to Table 1, such a configuration is critical for both leg members and diagonal (I) members located in zones (1) to (5). Fig. 11(a) shows a simulation for the tower as a vertical beam located in a vertical plane parallel to the conductors. The loads acting on this beam due to both the considered downburst configuration and normal wind loading corresponding to  $\theta_f = 90^\circ$  are shown in Fig. 11(a). These loads are drawn to scale using the scaling ratio provided in the figure. It can be noticed from the two plots shown in Fig. 11(a) that the two sets of loading are almost identical. The only exception is that the downburst case leads to point loads having relatively small amplitudes and acting at the conductors and the ground wires locations. These loads represent the result from a situation leading to unbalanced axial forces developing at conductors located at opposite sides of the tower. The offset between the centres of

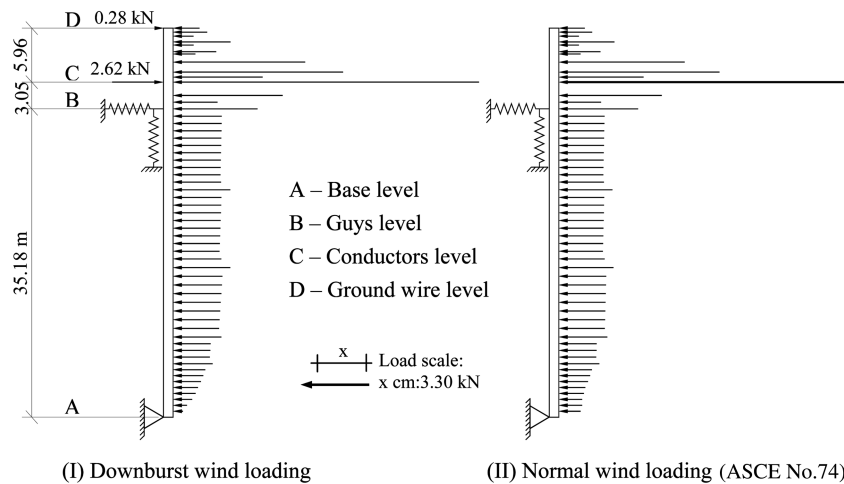


Fig. 11(a) Vertical profile of wind loading at  $\theta_f = 90^\circ$

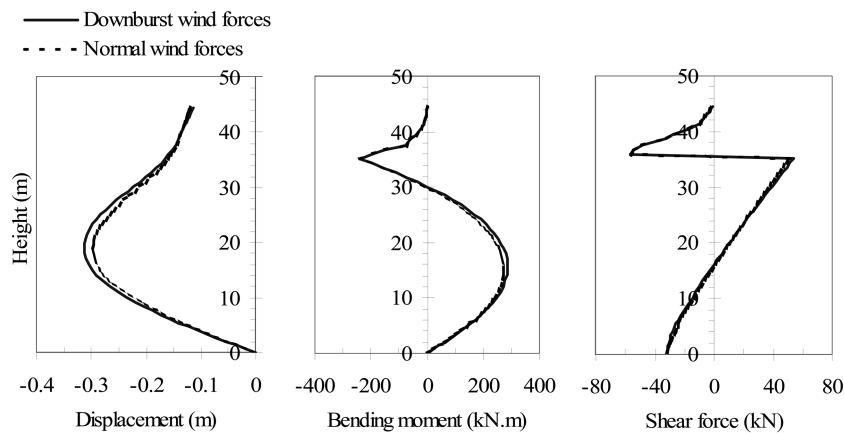


Fig. 11(b) Structural behaviour at  $\theta_f = 90^\circ$

the downburst and the tower as well as between the centre of the tower and the conductors lead to this unbalanced set of loads. Fig. 11(b) shows the displacement profile as well as the bending moment and shear force diagrams along the height of the equivalent beam for both the downburst and normal wind load cases. Due to the similarity in loading, the three diagrams are almost identical for both the downburst and normal wind cases. Results provided in Table 1 indicate that the axial forces in leg and diagonal (I) members located in zones (1) to (5), which are governed by this downburst configuration, have almost equal values for both the downburst and the normal wind load cases. This finding can be explained in view of the almost identical diagrams shown in the three plots provided in Fig. 11(b). By comparing the bending moment diagrams for the downburst cases provided in Fig. 10(b) and 11(b), it can be seen that larger positive moment values are obtained for the  $\theta_f = 90^\circ$  case. This explains why the critical downburst configurations for the leg members of zones (1) and (5) involved this angle value.

### 6.3. Case II ( $\theta_f = 30^\circ$ )

As shown in Table 1, intermediate values for  $\theta_f$  led to maximum forces in many members of zones (6) and (7). As an illustration, this case consider the behaviour of the tower under the following downburst configuration;  $D_{ff} = 1000$  (m),  $r_f/D_{ff} = 1.60$ ,  $\theta_f = 30^\circ$  and  $V_{ff} = 70.0$  (m/s). Fig. 12 shows the distribution of transverse load acting on six conductors located at both sides of the tower due to both downburst and normal wind loads. The uneven distribution of the forces associated with the downburst case is obvious in the figure. Meanwhile, it is clear that the loads acting on the left side of the tower (side adjacent to the downburst) are much larger than the loads associated with normal winds. As a result of the uneven distribution of the downburst loading, the reactions at the target tower will involve both transverse and longitudinal components associated with the large deformation behaviour of the conductors. Fig. 12(b) shows a simulation of the conductor cross-arm as a beam fixed to the tower. Loads acting on the simulated beam as a result of both the downburst and the normal wind loadings are shown in the figure. It is clear that the loads acting on the cross-arm itself are quite small and that the behaviour will be governed by the large loads acting on the conductors. As shown in the figure, axial loads having a magnitude of 27.40 kN and 15.0 kN act along the transverse direction of the conductors as a result of the downburst and the normal wind cases, respectively. On the other hand, a load of 60.10 kN acts along the longitudinal direction of the conductors as a result of the unbalanced downburst forces shown in Fig. 12(a). This large unbalanced force, which occurs only during downburst located at intermediate angles  $0^\circ < \theta_f < 90^\circ$ , explains why the maximum internal forces in many members of zones (6) and (7) exceed significantly those due to normal wind loading. In general, the results shown in Table 1 indicate that for the region bounded by the bottom support and the guys, the ASCE No.74 guidelines (1991) for normal wind loading leads to internal forces that are almost equal to those resulting from the critical downburst configuration. This is true with the exception of few members that are subjected to small values of internal forces. On the other hand, it is clear that the internal forces developing in the cross-arm area due to critical downburst configuration significantly exceed those due to normal wind loads.

## 7. Conclusions

A detailed study has been conducted to assess the performance of guyed transmission towers

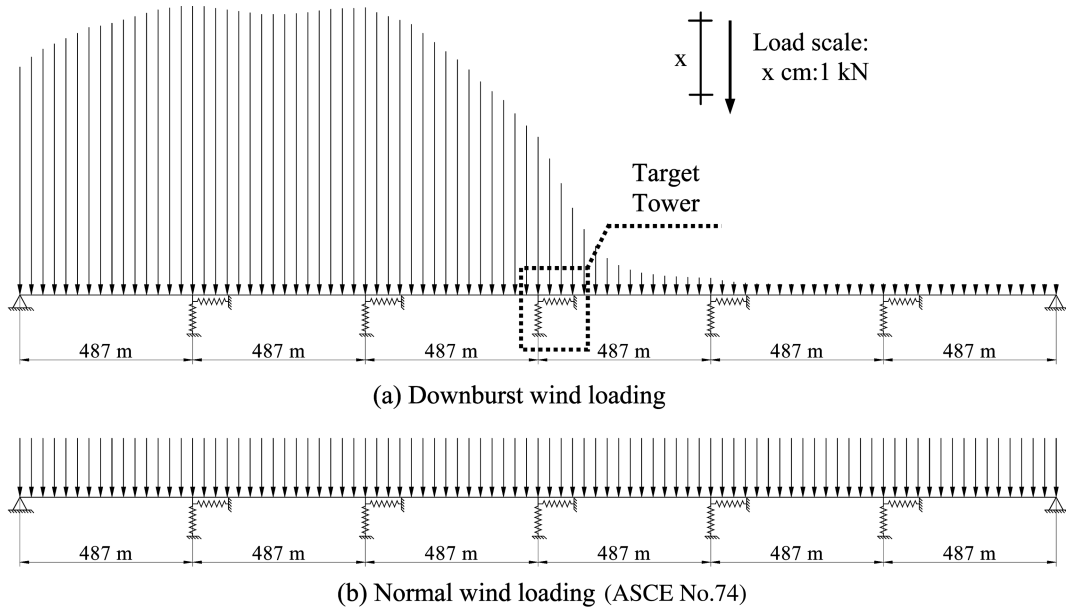


Fig. 12(a) Horizontal projection of wind loading for  $\theta_f = 30^\circ$  on six spans of the transmission line

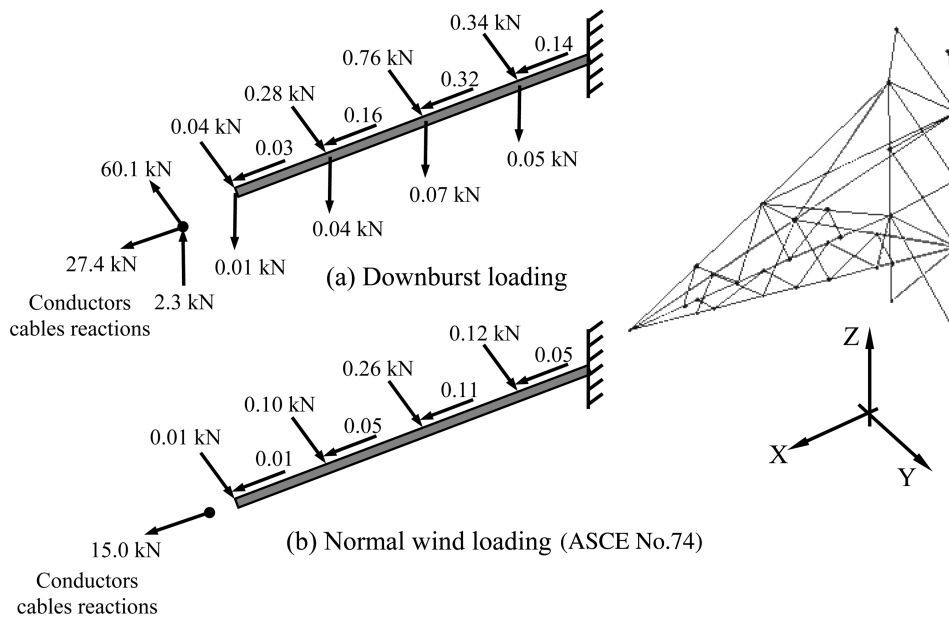


Fig. 12(b) Loads acting on the conductors cross-arm at  $\theta_f = 30^\circ$

under loads resulting from downburst events. Loads acting on a structure due to a downburst depend on the jet diameter  $D_{jf}$  of the event and the radial coordinate of its centre ( $r_f$  and  $\theta_f$ ) relative to the centre of the tower. The extensive parametric study involved variations of the three parameters. The first part of the study focused on describing the variation of the radial and vertical velocity components of the downburst flow field with the downburst parameters. The following

conclusions can be drawn from this part of the study.

For the same  $r_f/D_{Jf}$  ratio, the variation of maximum and minimum values of radial velocity component with  $D_{Jf}$  is very small, while the variation of the steady state value is more significant.

The values of the time of occurrence of maximum and minimum values of radial velocity component are almost linearly proportional to  $D_{Jf}$ . The time of occurrence of the maximum value of the radial velocity component ranges between  $(0.196 \sim 0.232) D_{Jf}$ , while it ranges between  $(0.225 \sim 0.267) D_{Jf}$  for the minimum value.

The downburst with configuration  $r_f/D_{Jf} = 1.20$  and  $D_{Jf} = 250$  (m) produces the largest values of horizontal forces acting on the tower.

The maximum, minimum, and steady state values of axial velocity component decrease with the increase of  $D_{Jf}$ .

The time of occurrence of maximum and minimum values of the axial velocity component is linearly proportional to  $D_{Jf}$ . For the maximum value of axial velocity component, the time of occurrence ranges between  $(0.190 \sim 0.225) D_{Jf}$ , while for the minimum value, it ranges between  $(0.197 \sim 0.246) D_{Jf}$ .

- The wind field associated with the radial component has velocity magnitudes that significantly exceed those associated with the axial component.

The second part of the study assesses the variations of the members' internal forces with the change of downburst characteristics. The value of  $\theta_f = 0^\circ$  corresponds to the case where the centre of the tower and the centre of the downburst are located in a vertical plane perpendicular to the transmission line, while the value  $\theta_f = 90^\circ$  corresponds to the case where the centre of the tower and the centre of the downburst are located in a vertical plane parallel to the transmission line. Also, it should be noted that diagonal (I) members are located in a vertical plane parallel to the transmission line, while diagonal (II) members are located in a vertical plane normal to the transmission line. The following conclusions can be drawn from this part of the study:

- *Tower region underneath the supporting guys*

- For the leg members, the axial forces slightly change with the angle  $\theta_f$  with maximum values occurring at  $\theta_f = 90^\circ$ .
- For the diagonal members, the maximum axial force develops in each member when the plane containing the centres of the downburst and the tower is parallel to that member.
- For both the leg and diagonal members, maximum axial forces happen at  $r_f/D_{Jf} = 1.20$ . Also, the axial forces in these members show a monotonic decrease with the increase of the jet diameter  $D_{Jf}$ .

- *Tower region of the guys and the conductors cross-arms.*

- The absolute maximum values of axial forces in both the leg and the diagonal (I) members occur at  $\theta_f = 45^\circ$ .
- For the cases where the maximum forces happen at intermediate value of  $\theta_f$  (i.e.  $\theta_f \neq 0^\circ$  and  $\theta_f \neq 90^\circ$ ), the corresponding  $r_f/D_{Jf}$  ratio is different than the value of 1.20 that was consistently shown to be critical for the rest of the tower.
- The peak values of the axial forces occur at  $D_{Jf} = 500$  (m) and (1000) for diagonal (I) and diagonal (II) members, respectively.

- *Guys and conductors cross-arms*

- An intermediate value of  $\theta_f = 30^\circ$  leads to maximum forces in the members of this region.
- The maximum forces in members located in the guys and conductors cross-arms occur at  $r_f/D_{Jf}$  ratio of 1.40 and 1.60, respectively. Also, the critical values of the jet diameter  $\theta_f$  for these members varied between 500 (m) and 1000 (m) for guys and conductors cross-arms, respectively.

In general, the results of current study show that designing the part of guyed transmission towers located underneath the supporting guys according to the ASCE No.74 guidelines is adequate to resist loads associated with downbursts. However, special consideration to downburst loading must be taken into account when designing the region of the tower where the guys and the conductors cross-arms are located. A design according to normal wind conditions in this region might not be conservative to sustain loads associated to downburst events.

## Acknowledgements

The authors are obliged to the Natural Sciences and Engineering Research Council of Canada (NSERC) and Manitoba Hydro Company, Canada, for the financial and in-kind supports provided to this research work. Also, the authors deeply appreciate the SHARCNET supercomputer facility, and staff at the University of Western Ontario, Canada. Finally, the authors acknowledge Prof. H. Hangan and Dr. J-D. Kim for their efforts in providing the downburst wind data.

## References

- American Society of Civil Engineers (ASCE) (1991), "Guidelines for electrical transmission line structural loading", *ASCE Manuals and Reports on Engineering Practice*, No. 74, NY.
- Chay, M. T., Albermani, F. and Wislon, R. (2006) "Numerical and analytical simulation of downburst wind loads", *Eng. Struct.*, **28**, 240-254.
- Chen, L. and Letchford, C. (2003). "Parametric study on the response of the CAARC building to downbursts in the time domain", *Proceedings of 11<sup>th</sup> International Conference on Wind Engineering*, Lubbock, Texas, Electronic Version.
- Engineering and Construction, Manitoba Hydro (1991). "Direct current guyed suspension tower type A-402-0 structural steel layout", *Transmission Line Standard*, 1-30000-DE-25111-0002.
- Gerges, R. R. and El-Damatty, A. A. (2002), "Large displacement analysis of curved beams", *Proceedings of CSCE Conference*, Montreal, QC, Canada, ST 100.
- Hangan, H., Roberts, D., Xu, Z. and Kim, J. (2003), "Downburst simulation. Experimental and numerical challenges", *Proceedings of 11<sup>th</sup> International Conference on Wind Engineering*, Lubbock, Texas, Electronic Version.
- Holmes, J. D. and Oliver, S. E. (2000), "An empirical model of a downburst", *Eng. Struct.*, **22**, 1167-1172.
- Ivan, M. (1986), "A ring-vortex downburst model for flight simulations", *J. Aircraft*, **23**, 232-236.
- Koziey, B. and Mirza, F. (1994), "Consistent curved beam element", *Comp. Str.*, **51**(6), 643-654.
- Li, C. Q. (2000), "A stochastic model of severe thunderstorms for transmission line design", *Prob. Eng. Mech.*, **15**, 359-364.
- Savory, E., Parke, G., Zeinoddini, M., Toy, N. and Disney, P. (2001), "Modelling of tornado and microburst-induced wind loading and failure of a lattice transmission tower", *Eng. Struct.*, **23**, 365-375.
- Shehata, A. Y., El Damatty, A. A. and Savory, E. (2005), "Finite element modelling of transmission line under downburst wind loading", *Finite Element Analysis Design*, **42**, 71-89.
- Transmission and Civil Design Department, Manitoba Hydro (1999), "Bipole 1 & 2 HVDC Transmission Line Wind Storm Failure on September 5, 1996 – Review of Emergency Response, Restoration and Design of These Lines", 98-L1/1-37010-06000, 54 pp.
- Vicory, D. D. (1992), "Assessment of microburst models for downdraft estimation", *J. Aircraft*, **29**, 1043-1048.
- Zhu, S. and Etkin, B. (1985), "Model of the wind field in a downburst", *J. Aircraft*, **22**, 595-601.